Scientific Research Associates, inc.

50 Nye Road, P.O. Box 1058
Glastonbury, Connecticut 06033
(203) 659-0333

REPORT NO. R88920028-F (a)

ANALYSIS OF THE SUBMARINE APPENDAGE FLOW FIELD

Ralph Levy
Assistant Vice-President

FINAL REPORT

Contract No. N000167-86-C-0048

Sponsored by:

Office of Naval Research
88 Quincy Street
Arlington, VA 22217

Under the Applied Hydrodynamics Research Program

Approved for public release; distribution unlimited.

August 1988

SECURITY CLASSIFICATION OF THIS PAGE

REPORT DOCUMENTATION PAGE

Form Approved OMB No. 0704-0188

1a. REPORT SECURITY CLASSIFICATION: Unclassified	1b. RESTRICTIVE MARKINGS
2a. SECURITY CLASSIFICATION AUTHORITY	3. DISTRIBUTION/AVAILABILITY OF REPORT: Approved for public release; distribution unlimited
2b. DECLASSIFICATION/DOWNGRADING SCHEDULE	
4. PERFORMING ORGANIZATION REPORT NUMBER(S): R88920028-F (a) (b)	5. MONITORING ORGANIZATION REPORT NUMBER(S)
6a. NAME OF PERFORMING ORGANIZATION: Scientific Research Associates; 6b. OFFICE SYMBOL (If applicable): 8N189	7a. NAME OF MONITORING ORGANIZATION: David Taylor Research Center
6c. ADDRESS (City, State, and ZIP Code): 50 Nye Road, P.O. Box 1058, Glastonbury, CT 06033	7b. ADDRESS (City, State, and ZIP Code): V.J. Monacella (Code 1504), Bethesda, MD 20084-5000
8a. NAME OF FUNDING/SPONSORING ORGANIZATION: Office of Naval Research; 8b. OFFICE SYMBOL (If applicable): Code 1215	9. PROCUREMENT INSTRUMENT IDENTIFICATION NUMBER: N00167-86-C-0048
8c. ADDRESS (City, State, and ZIP Code): 800 N. Quincy Street (J.Fein), Arlington, VA 22217	10. SOURCE OF FUNDING NUMBERS: PROGRAM ELEMENT NO. / PROJECT NO. / TASK NO. / WORK UNIT ACCESSION NO.

11. TITLE (Include Security Classification): Analysis of the Submarine Appendage Flow Field

12. PERSONAL AUTHOR(S): Ralph Levy

13a. TYPE OF REPORT	13b. TIME COVERED	14. DATE OF REPORT (Year, Month, Day)	15. PAGE COUNT
Final Report	FROM 4/86 TO 10/87	88/08/15	20

16. SUPPLEMENTARY NOTATION: Work sponsored under Office of Naval Research (AHR Program) Administered by David Taylor Research Center

17. COSATI CODES			18. SUBJECT TERMS (Continue on reverse if necessary and identify by block number)
FIELD	GROUP	SUB-GROUP	Applied Hydrodynamics Research Program; Submarine, Appendage, Hull-Sail, 3-D Viscous Flow

19. ABSTRACT (Continue on reverse if necessary and identify by block number)

The corner vortex originating in the hull-sail intersection region is an important component of the submarine flow field. The vortex may play a major role in overall drag, wake development and propeller performance, and may be a major acoustic source. The flow itself is a complex one, being three-dimensional, viscous and turbulent. Earlier work computed the flow field around the hull and the sail. The present report focuses on the portion of the flow in the hull-sail corner downstream of the sail leading edge. The paper first details the analysis which is based upon a three-dimensional, viscous, spatial forward marching approach. The solution procedure which is based upon ADI techniques is described. A comparison with the turbulent flow data of McMahon, Hubbartt and Kubendran (1983) is presented. The computer code used to run these calculations has been transmitted to the NRL Cray computer. A User's Manual for this code including sample input and output has been forwarded to David Taylor Research Center.

20. DISTRIBUTION/AVAILABILITY OF ABSTRACT	21. ABSTRACT SECURITY CLASSIFICATION	
☐ UNCLASSIFIED/UNLIMITED ☒ SAME AS RPT. ☐ DTIC USERS	Unclassified	
22a. NAME OF RESPONSIBLE INDIVIDUAL	22b. TELEPHONE (Include Area Code)	22c. OFFICE SYMBOL

DD Form 1473, JUN 86 *Previous editions are obsolete.* SECURITY CLASSIFICATION OF THIS PAGE

ANALYSIS OF THE SUBMARINE APPENDAGE FLOW FIELD

ABSTRACT

The corner vortex originating in the hull-sail intersection region is an important component of the submarine flow field. The vortex may play a major role in overall drag, wake development and propeller performance, and may be a major acoustic source. The flow itself is a complex one, being three-dimensional, viscous and turbulent. Earlier work computed the flow field around the hull and the sail. The present report focuses on the portion of the flow in the hull-sail corner downstream of the sail leading edge. The paper first details the analysis which is based upon a three-dimensional, viscous, spatial forward marching approach. The solution procedure which is based upon ADI techniques is described. A comparison with the turbulent flow data of McMahon, Hubbartt and Kubendran (1983) is presented. The computer code used to run these calculations has been transmitted to the NRL Cray computer. A User's Manual for this code including sample input and output has been forwarded to David Taylor Research Center.

Scientific Research Associates, inc.

50 Nye Road, P.O. Box 1058
Glastonbury, Connecticut 06033
(203) 659-0333

ANALYSIS OF THE SUBMARINE APPENDAGE FLOW FIELD

Ralph Levy
Assistant Vice-President

FINAL REPORT

Contract No. N000167-86-C-0048
Contract Amount $80,873

Sponsor:

V.J. Monacella
David Taylor Research Center
Code 1504
Bethesda, MD 22084-5000

Under the Advanced Hydrodynamics Research Program

August 1988

INTRODUCTION

The complex flow field of the submarine hull-sail interaction represents a difficult hydrodynamics problem which can be divided into four separate regions. The first region is the leading edge region of the sail where the adverse streamwise pressure gradient experienced by the oncoming hull boundary layer results in a complex three-dimensional flow separation ahead of the leading edge. Convection of this fluid around the leading edge sets up a horseshoe vortex. This flow has been analyzed by SRA under ONR sponsorship (Ref. 5). The second region is the hull/sail corner region where the interaction of the horseshoe vortex with the hull and sail boundary layers is of importance and is dominated by streamwise convection and transverse dissipation of vorticity. The third region contains the tip vortex shed off the top of the sail. The fourth region contains the wake of the sail and downstream wake-vortex-hull interactions.

All four regions contain complex fluid flow patterns in which streamwise vortices and viscous effects play major roles. In the case of the submarine appendage problem, the generation of the horseshoe vortex in the sail leading edge and hull corner region and the subsequent development of the streamwise vorticity as it proceeds downstream have major effects in determining hull drag, wake development, and possible acoustic sources. In addition, this strong streamwise vorticity could impinge upon the propeller and influence the propeller performance. Clearly, a technique for predicting this complex flow field would be a major asset in understanding submarine hydrodynamics as well as a benefit to the design process.

In developing an analysis for this problem, several possibilities of varying complexity can be considered. These include semi-empirical analyses, inviscid analyses with viscous corrections and three-dimensional viscous analyses. Based upon an understanding of the flow field it appears that, in general, semi-empirical analyses cannot be used with confidence for this problem. The strong role played both by viscous effects and three-dimensional flow patterns makes any semi-empirical analysis an unlikely candidate as a general predictive procedure. Similarly, although inviscid analyses can yield realistic flow field predictions in cases where viscous effects are confined to thin layers in the vicinity of no-slip walls, purely inviscid analyses appear unsuitable for the present problem. The horseshoe vortex generation clearly

requires a viscous analysis for this part of the problem. Even downstream of the generation region, viscous effects play an important role in the prediction of diffusion and dissipation of the streamwise vortex and in the interaction of the vortex, sail wake and hull. Clearly, an appropriate analysis should be based upon three-dimensional, viscous methods.

In the approach presented here, an existing forward marching, three-dimensional, viscous flow, numerical prediction technique has been adopted to simulate the hull sail corner flow field. In this study the calculation is begun downstream of the leading edge region in which the horseshoe vortex originates. The horseshoe vortex at the initial plane of the present calculation has been modeled by constructing forced vortices whose location, strength and extent are input parameters in the viscous flow computer program. Earlier work under this contract, presented at the 16th International Symposium on Naval Hydrodynamics, (Ref. 2) computed the flow field around the hull and sail. The present report focuses on the portion of the flow in the hull-sail corner downstream of the sail leading edge.

The body of this report discusses the governing equations, solution techniques and initial conditions used. A comparison with the turbulent flow data of McMahon et al. (Ref. 1) is presented.

FORWARD MARCHING COMPUTATIONAL PROCEDURE

Governing equations are derived through approximations made relative to a curvilinear coordinate system fitted to and aligned with the flow geometry under consideration. The coordinate system is chosen such that the streamwise or marching coordinate either coincides with or is at least approximately aligned with a known inviscid primary flow direction as determined, for example, by a potential flow for the given geometry. Transverse coordinate surfaces must be approximately perpendicular to solid walls or bounding surfaces, since diffusion is permitted only in these transverse coordinate surfaces.

Equations governing primary flow velocity, U_p, and a secondary vorticity, Ω_n, normal to transverse coordinate surfaces are derived utilizing approximations which permit solution of the governing equations as an initial value problem, provided reversal of the composite streamwise velocity does not occur. Terms representing diffusion normal to transverse coordinate surfaces (in the streamwise direction) are neglected. Secondary flow velocities are

determined from scalar and vector surface potential calculations in transverse coordinate surfaces, once the primary velocity and secondary vorticity are known. With the computed velocity field, the pressure field associated with the velocity field can be determined.

Primary-Secondary Velocity Decomposition

In what follows, vectors are denoted by an overbar, and unit vectors by a caret. The analysis is based on decomposition of the overall velocity vector field, $\bar{U}$, into a primary flow velocity, $\bar{U}_p$, and a secondary flow velocity, $\bar{U}_s$. The overall or composite velocity is determined from the superposition

$$\bar{U} = \bar{U}_p + \bar{U}_s \tag{1}$$

The primary flow velocity is represented as

$$\bar{U}_p = U_p \hat{i}_p \tag{2}$$

where $\hat{i}_p$ is a known inviscid primary flow direction determined, for example, from an a priori potential flow solution for the geometry under consideration. A streamwise coordinate direction from a body fitted coordinate system could be used as an approximation to this potential flow direction. The primary velocity, $\bar{U}_p$, is determined from solution of a primary flow momentum equation. The secondary flow velocity, $\bar{U}_s$, is derived from scalar and vector surface potential denoted ϕ and ψ, respectively. If $\hat{i}_n$ denotes the unit vector normal to transverse coordinate surfaces, if ρ is density, and if ρ_o is an arbitrary constant reference density, then $\bar{U}_s$ is defined by

$$\bar{U}_s \equiv \nabla_s \phi + (\rho_0/\rho)\nabla x \hat{i}_n \psi \tag{3}$$

where ∇_s is the surface gradient operator defined by

$$\nabla_s = \nabla - \hat{i}_n(\hat{i}_n \cdot \nabla) \tag{4}$$

It follows that since $\hat{i}_n \cdot \bar{U}_s = 0$, then U_s lies entirely within transverse coordinate surfaces. Equation (3) is a general form permitting both rotational and irrotational secondary flows and will lead to governing equations which may be solved as an initial-boundary value problem. The overall velocity decomposition (1) can be written

$$\bar{U} = U_p \hat{i}_p + \nabla_s \phi + (\rho_0/\rho)\nabla x \hat{i}_n \psi \tag{5}$$

Surface Potential Equations

Equations relating ϕ and ψ with U_p, ρ, and the secondary vorticity component, Ω_n, can be derived using Eq. (5) as follows: From continuity,

$$\nabla \cdot \rho \bar{U} = 0 = \nabla \cdot \rho U_p \hat{i}_p + \nabla \cdot \rho \nabla_s \phi + \rho_0 \nabla \cdot \nabla x \hat{i}_n \psi \tag{6}$$

and from the definition of the vorticity, Ω_n, based on the secondary flow within the transverse surfaces

$$\hat{i}_n \cdot \nabla x \bar{U} \equiv \Omega_n = \hat{i}_n \cdot \nabla x U_p \hat{i}_p + \hat{i}_n \cdot \nabla x (\rho_0/\rho) \nabla x \hat{i}_n \psi + \hat{i}_n \cdot \nabla x \nabla \phi_s \tag{7}$$

Since the last term in each of Eqs. (6) and (7) is zero by vector identity, Eqs. (6) and (7) can be written as

$$\nabla \cdot \rho \nabla_s \phi = -\nabla \cdot \rho U_p \hat{i}_p \tag{8}$$

$$\hat{i}_n \cdot \nabla x (\rho_0/\rho) \nabla x \hat{i}_n \psi = \Omega_n - \hat{i}_n \cdot \nabla x U_p \hat{i}_p \tag{9}$$

Note that the last term in Eq. (9) is identically zero in a coordinate system for which $\hat{i}_n$ and $\hat{i}_p$ have the same direction, and would be small if $\hat{i}_n$ and $\hat{i}_p$ are approximately aligned. In any event, given a knowledge of U_p, Ω_n and ρ, the surface potentials ϕ and ψ can be determined by a two-dimensional elliptic calculation in transverse coordinate surfaces at each streamwise location. In turn, $\bar{U}_s$ can be computed from Eq. (3), and the composite velocity $\bar{U}$ will satisfy continuity. Equations for U_p and Ω_n are obtained from the equations governing momentum and vorticity, respectively.

The streamwise momentum equation is given by

$$\hat{i}_p \cdot [(\bar{U} \cdot \nabla)\bar{U} + (\nabla P)/\rho] = \hat{i}_p \cdot \bar{F} \tag{10}$$

where P is pressure and ρF is force due to viscous stress and terms in F representing streamwise diffusion are neglected. The pressure term in the streamwise momentum Eq. (10) can be taken from a simpler analysis such as an inviscid flow analysis. While this results in a set of equations which can be solved by forward marching, the surface pressures which are due to the pressure field imposed upon the flow are the inviscid flow pressures. Since the actual surface pressures are often of primary interest, a new estimate of the actual surface pressure which includes viscous and secondary flow effects can be computed from the resulting velocity field in the following manner.

The momentum equations in the transverse surfaces are:

$$\begin{aligned} \hat{i}_1 \cdot [(\rho\bar{U} \cdot \nabla)\bar{U} + \nabla P - \rho\bar{F}] &= 0 \\ \hat{i}_2 \cdot [(\rho\bar{U} \cdot \nabla)\bar{U} + \nabla P - \rho\bar{F}] &= 0 \end{aligned} \tag{11}$$

Equation (11) represents components of the momentum vector in the transverse surfaces:

$$\begin{aligned} \hat{i}_1(\hat{i}_1 \cdot [(\rho\bar{U} \cdot \nabla)\bar{U} + \nabla P - \rho\bar{F}]) &= 0 \\ + \hat{i}_2(\hat{i}_2 \cdot [(\rho\bar{U} \cdot \nabla)\bar{U} + \nabla P - \rho\bar{F}]) &= 0 \end{aligned} \tag{12}$$

The divergence of this vector can be written as a Poisson equation for the pressure P at each transverse surface:

$$\begin{aligned} \nabla_s^2 P = \nabla_s^2 (P_I + P_c) = &- \frac{\partial}{\partial x_1} (\hat{i}_1 \cdot [(\rho\bar{U} \cdot \nabla)\bar{U} - \rho\bar{F}]) \\ &- \frac{\partial}{\partial x_2} (\hat{i}_2 \cdot [(\rho\bar{U} \cdot \nabla)\bar{U} - \rho\bar{F}]) \end{aligned} \tag{13}$$

where P_I is the imposed pressure, P_c is a viscous correction to the pressure field and x_1 and x_2 are coordinates in the $\hat{i}_1$ and $\hat{i}_2$ directions, respectively. Equation (13) can be solved for the pressure correction, P_c, at each computational station using Neuman boundary conditions derived from

Eq. (12). The use of Neuman boundary conditions requires an additional parameter which is only a function of the normal direction, $P_v(x_3)$, in order to set the level of the pressure field. For external flows, $P_v(x_3)$ is set to match the imposed pressure at an appropriate far field location.

Secondary Vorticity

The equation governing Ω is obtained by cross differentiating each of the transverse momentum equations (11). Eliminating the pressure in the two equations results in a single equation for the transport of the vorticity normal to the transverse surface. This equation has the form

$$\bar{U}\cdot\nabla\Omega_n - \bar{\Omega}\cdot\nabla U_n = G_n + C \tag{14}$$

where G_n is the normal component of

$$\bar{G} = \nabla\times\bar{F} \tag{15}$$

and C is a collection of curvature terms arising from changes in orientation of the transverse surface as a function of streamwise coordinate.

Governing System of Equations

A complete system of five coupled equations governing U_p, Ω_n, ϕ, ψ, and P is given by Eqs. (8), (9), (10), (14) and (13). Ancillary relation Eq. (5) is given for the composite velocity. In Ref. 2, these equations are given in general orthogonal coordinates and in Ref. 3 in nonorthogonal coordinates.

Numerical Method

Since techniques for obtaining the basic inviscid flow solution are well known and numerous, they need not be enumerated or discussed here. Instead, the present development concentrates on describing the numerical method used to solve the system of governing equations. Streamwise derivative terms in the governing equations have a form such as $u_3\partial(\ )/\partial x_3$, and because the streamwise velocity u_3 is very small in the viscous dominated region near no-slip walls, it is essential to use implicit algorithms which are not subject to stringent

stability restrictions unrelated to accuracy requirements. Although it is possible to devise algorithms for solution of the governing equations as a fully coupled implicit system, such algorithms would require considerable iteration for the system of equations treated here, and this would detract from the overall efficiency. The present method seeks to reduce the amount of iteration required and yet avoid the more severe stability restrictions of explicit algorithms. The method partitions the system of governing equations into subsystems which govern the primary flow, the secondary flow, and the turbulence model. The primary-flow subset of equations contains the streamwise momentum equation. The secondary-flow subset of equations contains the secondary vorticity equation, the scalar and vector potential equations and the pressure equation. These subsystems are decoupled by linearizing the solution variables in the spatial marching direction.

Summary of Algorithm

The governing equations are replaced by finite-difference approximations. Three-point central difference formulas are used for all transverse spatial derivatives. Analytical coordinate transformations are employed as a means of introducing a nonuniform grid in each transverse coordinate direction to concentrate grid points in the wall boundary layer regions. Second-order accuracy for the transverse directions is rigorously maintained. Two-point backward difference approximations are used for streamwise derivatives, although this is not essential.

The primary flow subsystem of viscous equations is solved via a scalar ADI scheme. In this application this is the streamwise momentum equation. Given the solution for the primary flow, the secondary flow subsystem can be solved. First, the scalar potential equation (continuity) is solved using a scalar iterative ADI scheme. Next, the secondary vorticity and vector potential equations are written as a fully implicit coupled system and solved using an iterative linearized block implicit (LBI) scheme (cf. Briley and McDonald, Ref. 3). In selecting boundary conditions for the secondary flow subsystem, care must be taken to ensure that the final secondary velocity satisfies the no-slip condition accurately. Zero normal derivatives of ϕ are specified in the scalar potential equation, and this boundary condition corresponds to zero normal velocity. It is not possible to simultaneously specify the tangential

velocity, however, and thus the ϕ-contribution to the secondary velocity will have a nonzero tangential (slip) component, denoted v_t, at solid boundaries. In the coupled vorticity and vector-potential equations, both normal and tangential velocity components can be specified as boundary conditions, since these equations are solved as a coupled system. By choosing (a) zero normal velocity, and (b) $-v_t$ as the ψ-contribution to the tangential velocity, the slip velocity v_t arising from the ϕ calculation is cancelled, and the composite secondary flow velocity including both ϕ and ψ contributions will satisfy the no-slip condition exactly.

A summary of the overall algorithm used to advance the solution a single axial step follows. It is assumed that the solution is known at the n-level x^n and is desired at x^{n+1}.

(1) The imposed streamwise pressure gradient distribution is determined from an a priori inviscid potential flow.

(2) The momentum equation is solved using an iterative scalar ADI scheme to determine u^{n+1}.

(3) Using values now available for u^{n+1}, the scalar potential equation (8) is solved using an iterative scalar ADI scheme to obtain ϕ^{n+1}. This ensures that the continuity equation is satisfied.

(4) The equations for vorticity (14) and vector potential (9) form a coupled system for Ω^{n+1} and ψ^{n+1}, which is solved as a coupled system using an iterative LBI scheme.

(5) Values for the transverse velocities v_s and w_s are computed from Eq. (3).

(6) Using the computed velocity field, the transverse pressure field is computed from Eq. (13) by an iterative scalar ADI scheme.

Boundary Conditions for the Hull-Sail Flow Computations

The hull surface and the sail surface are no-slip walls. On these boundaries the no-slip condition was satisfied by setting the normal gradient of the scalar potential (the normal velocity) to zero. In the coupled vector potential and vorticity equations the normal component of the rotational velocity was set to zero and the tangential component was set equal and opposite to the tangential component of the velocity generated by the scalar potential. These conditions allowed an implicit specification of the vector

potential and the vorticity on the no-slip boundary, as discussed above in the summary of the algorithm. The resultant secondary velocity field satisfies the no-slip conditions on the boundary. The streamwise velocity was also set to zero at the solid boundary.

Far field conditions were specified on the other two boundaries. The streamwise velocity was extrapolated from the interior flow field. The scalar potential was set to a constant so that the tangential component of the irrotational velocity was zero. This condition allowed outflow through the boundary due to the displacement effect of the boundary layers. The vector potential was set to zero so that the normal component of the rotational velocity is zero. The streamwise vorticity was set to zero.

Initial Vortex Specification

Hull and sail boundary layer thicknesses are specified. Outside these boundary layers the streamwise velocity is set to unity. Within the boundary layers, the velocity profiles corresponding to flat plate boundary layers at the appropriate Reynolds numbers are used. As in Reference 2, near the hull-sail corner, where the two boundary layers merge, an effective boundary layer is approximated at a point in the flow from:

$$\left(\frac{y}{\delta}\right)_{eff} = \left(\left(\frac{\delta_H}{y_H}\right)^{3/2} + \left(\frac{\delta_S}{y_S}\right)^{3/2} \right)^{-2/3} \qquad (16)$$

where δ_H and δ_S are the hull and sail boundary layer thickness and y_H and y_S are the distance to the hull and sail. This empirical relation was found to reproduce the boundary layer profile in a corner without a forced vortex.

The initial vortex distribution is determined by a two-step procedure: first setting a vortex strength and then solving vorticity-streamfunction equations in the initial cross plane to create a starting secondary flow that is compatible with the hull-sail corner. This is accomplished by first constructing forced vortices whose strength, location and core size are specified through input to the code. The strength and extent of the vortex is first calculated from

$$\Omega = 2\,\frac{q}{r} \qquad (17)$$

where Ω, the vorticity, is determined as a constant function of q, the magnitude of the rotational velocity at the edge of the core, and r, the radius of the forced vortex core. Everywhere outside this forced vortex the vorticity is initially set to zero. Second, this constructed vorticity distribution is modified through solution of equations governing streamwise vorticity transport and governing the vector potential in the initial transverse plane subject to appropriate wall boundary conditions. Solution of these equations results in a new, modified vorticity distribution which includes the effect of the hull and the sail walls upon the initial plane vorticity profile.

Turbulence Model

In the high Reynolds number flows addressed in this report it is necessary to specify a turbulence model. Although one of the more sophisticated models, such as a multi-equation model, may eventually be necessary to obtain quantitative simulations, at present, a simpler mixing length type model is used in the analysis. The mixing-length turbulence model employed here computes an eddy viscosity (μ_T) based upon a mixing length distribution.

$$\frac{\mu_T}{Re} = \rho \ell^2 \left(2\bar{\bar{e}}:\bar{\bar{e}}\right)^{1/2} \tag{18}$$

where $\bar{\bar{e}}$ is the mean flow rate of strain tensor

$$\bar{\bar{e}} = \frac{1}{2}\left((\nabla\bar{U}) + (\nabla\bar{U})^T\right) \tag{19}$$

The mixing length (ℓ) is determined from the empirical relationship of McDonald and Camarata (Ref. 4) for equilibrium turbulent boundary layers.

$$\ell(y) = 0.09\delta_b \tanh\left[\kappa y/(0.09\delta_b)\right]D \tag{20}$$

where δ_b is the local boundary layer thickness, κ is the von Karman constant taken as 0.43, y is the distance from the wall and D is a sublayer damping factor

$$D = p^{1/2}(y^+ - \bar{y}^+)/\sigma \tag{21}$$

where p is the normal probability function, $y^+=y(\tau/\rho)^{1/2}/(\mu/\rho)$, τ is local shear stress, $\bar{y}^+ = 23$, and $\sigma = 8$. δ_b is taken as the average of the hull and sail boundary layer thickness and (y/δ) is computed from Eq. (16).

Test Case

The configuration of Ref. 1 is a thin, constant thickness strut normal to the floor of a wind tunnel. Incident flow along the floor of the wind tunnel strikes the rounded leading edge of the strut at zero angle of attack. A horseshoe vortex is formed at the leading edge and is convected downstream along the strut-floor corner. Since the flow in the leading edge region is elliptic, containing reversals in the streamwise flow and a stagnation line in the region of the strut leading edge, it is not appropriate to apply the spatial forward marching analysis to this region of the flow. Calculations were started aft of the strut leading edge and continued down the strut-floor corner to the downstream measuring stations.

McMahon, et al. measured flow velocities in transverse planes at three locations along the strut: 7.5 mm, 155 mm and 905 mm. The preferred method of starting the calculations would have been to take the measured conditions at the 7.5 mm station as the initial conditions. This was not possible since the measurements did not extend to near the strut.

Calculations were started upstream of the 7.5 mm measuring station and initial conditions were specified to try to match the measured flow at the 7.5 mm location. The location of the center of the forced vortex was set at 23 mm from the strut, as observed by the authors of Ref. 1. The vortex center was placed 7.7 mm from the floor. This was approximately 1/3 of the floor boundary layer thickness. The intensity of the initial vortex was set to try to establish a secondary flow pattern that was consistent with the measured flow. A series of calculations were run with variations in these initial parameters. As expected, the subsequent flow development, especially the amount of distortion of the floor boundary layer, was dependent on the strength of the initial vortex. The downstream location of the vortex was found to be insensitive to modest changes (+ 50%) in the initial vortex intensity. Other initial value parameters, such as strut boundary layer thickness and initial vortex location, were found to have only a weak influence on the computed flow at the downstream measuring stations.

The calculation was run on a 49×49 transverse coordinate grid that was clustered near the walls. The horizontal grid extended 200 mm from the strut with the first grid point .1 mm from the strut. The vertical grid extended 160 mm from the floor with the first grid point .03 mm from the floor. In each case, the first computational grid point off the solid surface was placed at a value of $y^+ < 10$. The streamwise step size started at 8.11 mm and increased at each step by a factor of 1.04. The first measuring station, 7.5 mm, occurred at step 5, permitting any starting problems to decay before the first measuring station. Subsequent measuring stations occurred at step 12 (165 mm) and step 33 (905 mm). The entire calculation used approximately 80,000 grid points and required approximately 2-1/2 minutes of CPU time on the NRL Cray computer.

Figures 1-3 present comparisons of the computed results with the data of McMahon, Hubbartt and Kubendran (Ref. 1). The distortion of the floor boundary layer by the horseshoe vortex is seen to be modelled fairly well by the calculation. Secondary flow patterns were also reproduced, although the secondary flow intensity appears to decay faster in the calculation than in the measurements. Although this decay could be attributable to limitations in the turbulence model, a larger source of uncertainty is the initial secondary flow near the strut. Initial upwards or downwards secondary flow along the strut would interact with the vortex to change the decay rate. The calculation used no initial vertical flow along the strut since there was no data to indicate the proper magnitude of this flow.

CONCLUSIONS

The long range objective of this study is to predict the flow field resulting from the hull-sail interaction of a submarine at angle of incidence. This includes the sail leading edge, the top of the sail, the hull-sail corner and the downstream sail wake-vortex-hull interactions. The first part of the study, reported in Reference 1, computed the flow around the hull and sail, starting aft of the sail leading edge. This report covering the second part of this study, documents the application of an efficient spatial marching, three-dimensional, viscous flow analysis to the flow in the hull-sail corner at zero angle of incidence. The calculations were started with an assumed forced vortex in the hull-sail corner aft of the sail leading edge and continued downstream to the last measuring station of McMahon et al. (Ref. 1). The computations are economical compared to computing solutions to the full

Navier-Stokes equations for this region. Computer run time on a Cray XMP using a single processor for 80,000 grid points is approximately 2-1/2 minutes for the calculation presented.

Further development of this analysis is needed to compute flow about a submarine at incidence including both pitch and yaw. To accomplish this the computations should incorporate (i) an imbedded Navier-Stokes solution to the sail leading edge, (ii) an a priori pressure field to improve quantitative accuracy, and (iii) a turbulence model suitable for wake flows. Benchmark quality experimental data will be necessary to verify the accuracy of the computational analysis.

The computer code used to run these calculations has been transmitted to the NRL Cray computer. A User's Manual for this code, including sample input and output, is included as the appendix of this report.

REFERENCES

1. McMahon, H., Hubbartt, J. and Kubendran, L.: Mean Velocities and Reynolds Stresses in a Juncture Flow, NASA CR-3695, 1983.

2. Levy, R. and Shamroth, S.J.: Numerical Analysis of the Viscous Flow Field Resulting from a Hull-Sail Interaction, 16th International Symposium on Naval Hydrodynamics, July 1986.

3. Briley, W.R. and McDonald, H.: On the Structure and Use of Linearized Block Implicit Schemes, Journal of Computational Physics, Vol. 34, 1980.

4. McDonald, H. and Camarata, F.J.: An Extended Mixing Length Approach for Computing the Turbulent Boundary Layer Development, Proceedings of the AFOSR-IFP - Stanford Conference on Boundary Layer Prediction, Stanford, CA, 1986.

5. Buggeln, R.C., Briley, W.R. and McDonald, H.: Solution of the Three-Dimensional Navier-Stokes Equations for a Turbulent Horseshoe Vortex Flow, SRA Report R87-920027-F, ONR, Contract N00014-85-C-0420, January 1987.

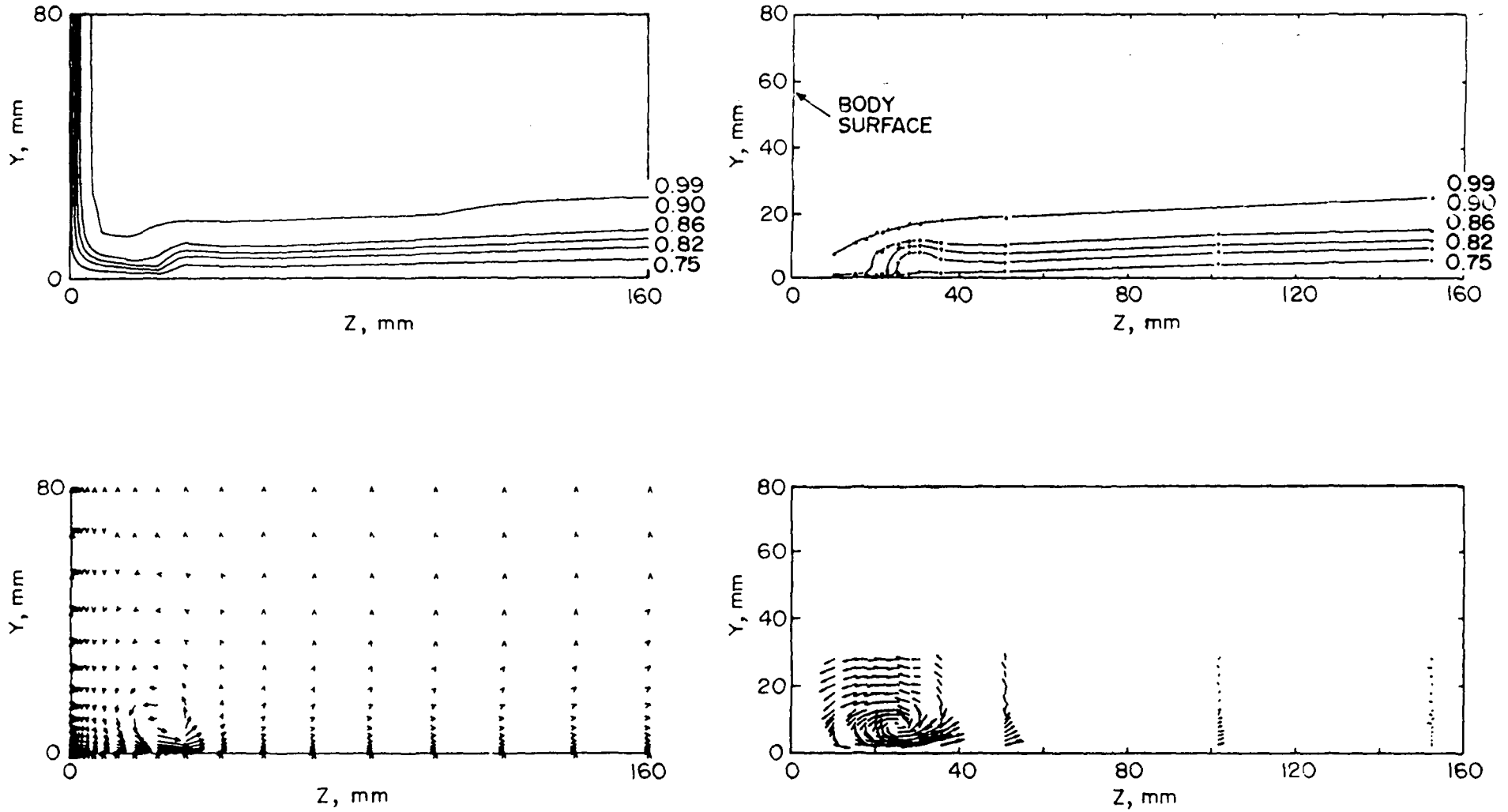

Figure 1. Comparison of Computed (left) and Measured (right) Velocities (ref. 1) at x = 76 mm.

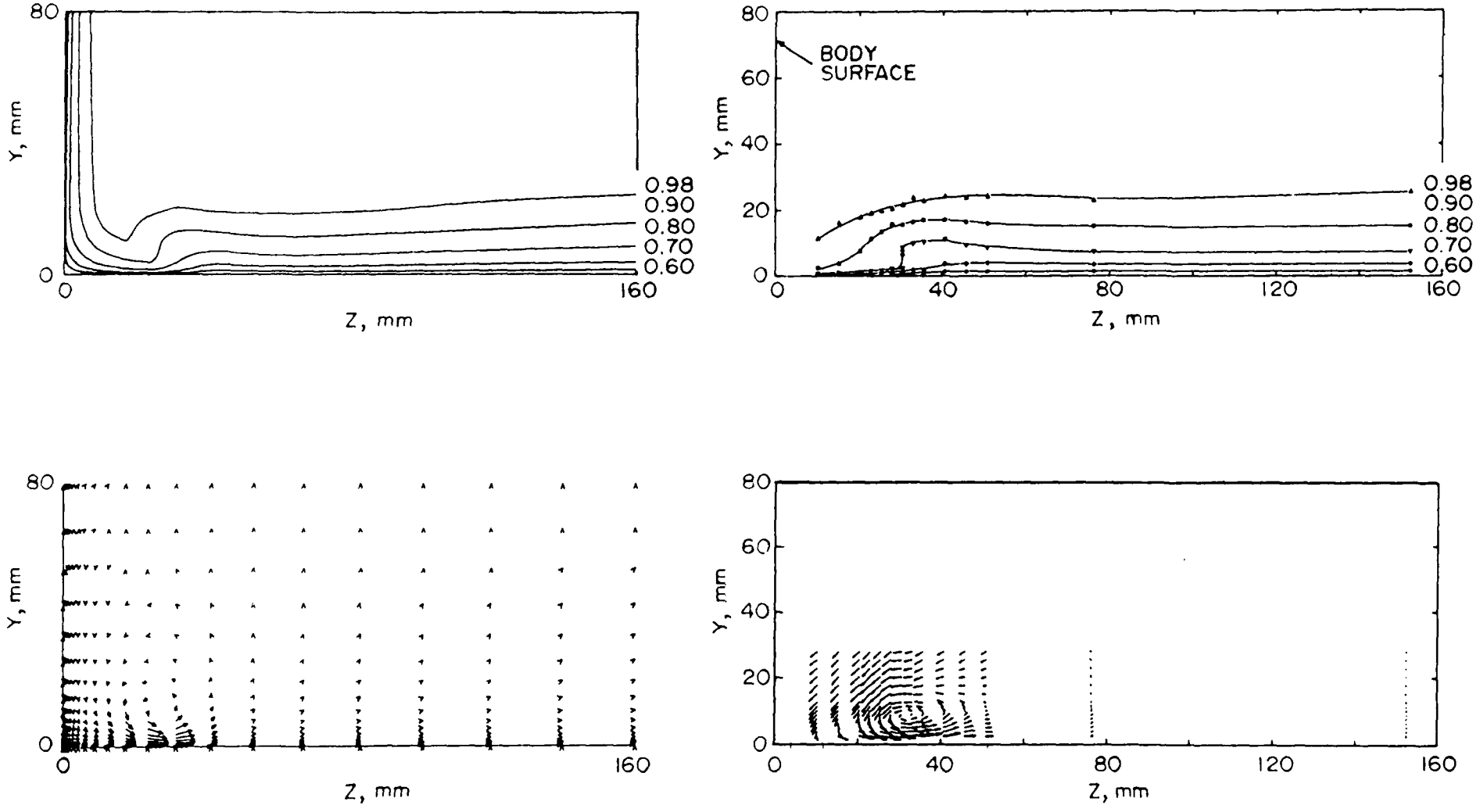

Figure 2. Comparison of Computed (left) and Measured (right) Velocities (ref. 1) at x = 165 mm.

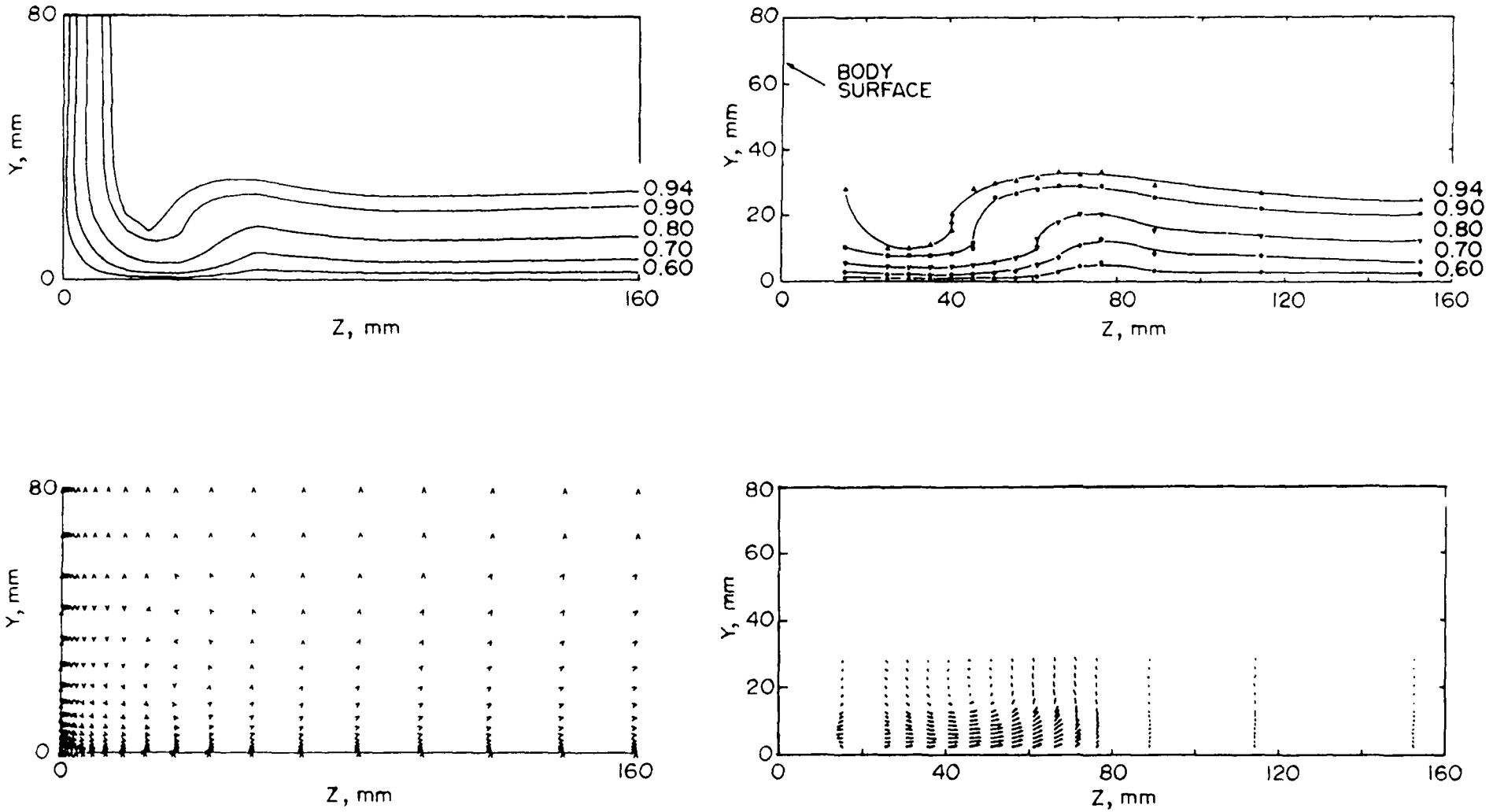

Figure 3. Comparison of Computed (left) and Measured (right) Velocities (ref. 1) at x = 902 mm.